Requirement for proper mitochondrial RNA processing in the restrictive control of cell proliferation during early lateral root morphogenesis

Kurataka Otsuka[1‡†], Akihito Mamiya[1†], Mineko Konishi[1§], Mamoru Nozaki[1‖], Atsuko Kinoshita[1¶], Hiroaki Tamaki[1#], Masaki Arita[1††], Masato Saito[1‡‡], Kayoko Yamamoto[1§§], Takushi Hachiya[2], Ko Noguchi[3], Takashi Ueda[4], Yusuke Yagi[5], Takehito Kobayashi[5‖‖], Takahiro Nakamura[5], Yasushi Sato[6], Takashi Hirayama[7], Munetaka Sugiyama[1*]

Affiliations:

[1]Botanical Gardens, Graduate School of Science, The University of Tokyo, Tokyo, 112-0001 Japan. [2]Department of Molecular and Functional Genomics, Interdisciplinary Center for Science Research, Shimane University, Shimane, 690-8504, Japan. [3]Department of Applied Life Science, School of Life Sciences, Tokyo University of Pharmacy and Life Sciences, Tokyo,192-0392, Japan. [4]Division of Cellular Dynamics, National Institute for Basic Biology, Aichi, 444-8585, Japan. [5]Department of Bioscience and Biotechnology, Faculty of Agriculture, Kyushu University, Fukuoka, 819-0395 Japan. [6]Biology and Environmental Science, Graduate School of Science and Engineering, Ehime University, Ehime 790-8577, Japan. [7]Institute of Plant Science and Resources, Okayama University, Okayama 710-0046, Japan.

[‡]Present address: Division of Molecular and Cellular Medicine, National Cancer Center Research Institute, Tokyo 104-0045, Japan. / R&D Division, Kewpie Corporation Sengawa Kewport, Tokyo 182-0002, Japan. / Division of Molecular and Cellular Medicine, Institute of Medical Science, Tokyo Medical University, Tokyo 160-0023, Japan. [§]Present address: Biotechnology Research Center, The University of Tokyo, Tokyo, 113-8657, Japan. [‖]Present address: Biotechnology Research Center and Department of Biotechnology, Toyama Prefectural University, Toyama, 939-0398, Japan. [¶]Present address: Department of Biological Sciences, Graduate School of Science, Tokyo Metropolitan University, Tokyo, Japan 192-0397 [#]Present address: Health and Crop Sciences Research Laboratory, Sumitomo Chemical Co. Ltd., Hyogo 665–8555, Japan. [‡‡]Present address: Innovation Promotion Division, Oji Holdings Corporation, Tokyo 135-8558, Japan. [§§]Present address: Department of Biological Sciences, Graduate School of Science, Tokyo, 113-0033, Japan. [‖‖]Present address: GRA&GREEN Inc., Incubation Facility 106, Nagoya University, Nagoya, 464-0814, Japan

[†]These authors contributed equally to this work.
[*]Corresponding author. Email: sugiyama@ns.bg.s.u-tokyo.ac.jp

Abstract:

Although mechanisms that activate organogenesis in plants are well established, much less is known about the local fine-tuning of cell proliferation, crucial for creating well-structured and sized organs. Here we show, through analysis of three temperature-dependent fasciation (TDF) mutants of *Arabidopsis*, *root redifferentiation defective 1* (*rrd1*), *rrd2*, and *root initiation defective 4* (*rid4*), that proper mitochondrial RNA processing is required for restrictive control of cell division during lateral root (LR) organogenesis. These mutants form abnormally broadened (i.e. fasciated) LRs under high-temperature conditions due to excessive cell division. We identified RRD1 as encoding a poly(A)-specific ribonuclease (PARN)-like protein and RRD2 and RID4 as encoding pentatricopeptide repeat (PPR) proteins. All TDF proteins were found to be involved in mitochondrial mRNA processing. Phenocopy of TDF mutants by respiratory inhibitors further corroborated our discovery. Our data provide novel insights into the molecular machinery and physiological and developmental roles of mitochondrial mRNA metabolism in plants.

Introduction

Plants elaborate their architecture by continuously developing new organs, such as leaves, floral organs, axillary stems and lateral roots (LR). Organogenesis begins with the local activation of cell proliferation in the plant body. In the following stages, proliferation is restricted to certain areas, which is essential for the formation of properly sized and structured organs, however, the molecular underpinnings of such regulation mostly remain unknown (*1*).

LRs serve as building blocks of the root system architecture, and are crucial for uptake and transport of water and minerals. The first visible step of LR formation occurs within the parent root, where a few cells start to divide, comprising the LR primordium. The LR primordium grows and eventually emerges out of the parent root to form a new LR (*2*). This process is closely described in the model plant *Arabidopsis thaliana*, making it one of the most ideal system to study the molecular mechanisms of organ development (*3*, *4*). In Arabidopsis, a small number of cells in a few adjacent files of the xylem pole pericycle layer, termed LR founder cells, re-enter the cell cycle and first divide in the anticlinal (perpendicular to the parental root axis) orientation (Fig. 1B) (*3*, *4*). Local accumulation of the phytohormone auxin is known to be critical for LR initiation, driving LR founder cell identity acquisition and division by degradation of the SOLITARY ROOT (SLR/IAA14) repressor, thus activating down-stream gene expression mediated by AUXIN RESPONSE FACTORS ARF7 and ARF19 (*5*). However, much less is understood about the coordinated periclinal (parallel to the surface of the root) and anticlinal divisions that subsequently take place. In particular, how cell proliferation becomes confined to the central zone of the primordium, giving rise to the dome-shaped structure largely remains a mystery (*2*), although requirement of several factors such as polar auxin transport (*6, 7*), control of auxin response (*8*), a few peptide hormones (*9*, *10*) and transcription factors (*11*, *12*), symplastic connectivity (*13*), epigenetic gene regulation (*14*) and mechanical interaction with overlaying tissue (*15*) have been revealed.

root redifferentiation defective 1 (*rrd1*), *rrd2*, and *root initiation defective 4* (*rid4*) are temperature-sensitive mutants of *Arabidopsis*, which we originally isolated by screening with adventitious root (AR) formation from hypocotyl tissue segments as an index phenotype (*16*, *17*). In addition to AR formation, other aspects of development, such as seedling growth and callus formation were also found to be affected at high temperature conditions (*16*, *17*). Most notable was their LR phenotype, in which abnormally broadened (i.e. fasciated) LRs were formed at 28°C (non-permissive temperature) but not at 22°C (permissive temperature) in a tissue culture setting, leading us to designate the three mutants as temperature-dependent fasciation (TDF) mutants (*18*). It was later revealed that early stages of LR development were likely affected in the TDF mutants and that the fasciated LRs formed exhibited exclusive enlargement of inner tissue (*18*), suggesting that the responsible genes for the TDF mutations (TDF genes) encode negative regulators of proliferation important for the size restriction of the central zone in early LR primordia formation, however, their molecular identity had been elusive.

Mitochondria are considered the “powerhouses” of the cell, supplying energy necessary for cellular activities. In comparison to other eukaryotes, RNA metabolism in mitochondria is particularly complex in plants, entailing numerous nucleus-encoded RNA-binding proteins (*19*). Given the relaxed nature of transcription, post-transcriptional processing, such as RNA editing, splicing, maturation of transcript

ends and RNA degradation, are known to play predominant roles in shaping the plant mitochondrial transcriptome (*19*). Although many factors participating in plant mitochondrial RNA processing have been identified, implications of their role in regulating plant development are limited so far (*19*).

Herein we report a detailed analysis of the TDF mutants. We established that LR fasciation in the TDF mutants are due to excessive cell division in early stages of LR formation. Next, we identified all three TDF genes as genes encoding nuclear-encoded mitochondrial RNA processing factors. Analysis of mitochondrial RNA demonstrated that RRD1 is involved in removal of poly(A) tails, and that both RRD*2* and RID4 are RNA editing factors. Defective protein composition of the mitochondrial electron transport chain was found in *rrd2* and *rid4*. Phenocopying of the TDF mutants by mitochondrial respiratory inhibition and reactive oxygen species (ROS) induction together with its reversal by ROS scavenging, suggested that ROS generation due to deficient RNA processing is the primary cause of excessive cell division during early LR development in the TDF mutants. Our discovery shed light on a new aspect of mitochondrial RNA processing relevant to controlling plant organogenesis.

Results

Effects of the TDF mutations on LR formation

To gain insight into fasciated LR formation in the TDF mutants, a detailed investigation was carried out using the semi-synchronous LR induction system (*20*), in which nearly de novo LR formation is induced from root explants of young seedlings upon culture in auxin-containing root inducing medium (RIM). In this system, a 6-day culture of TDF mutant explants results in high rates of LR fasciation at 28°C (non-permissive temperature) (Fig. 1A), but not at 22°C (permissive temperature) (*18*). To determine at which stage of LR formation do developmental abnormalities occur in the TDF mutants, LR primordium from earlier time-points were examined. In *Arabidopsis*, LR formation begins with anticlinal cell divisions in the xylem pole pericycle cell file, producing an array of short cells flanked by longer cells, which serves as the origin of the LR primordium (stage I; Fig. 1B) (*3*, *4*). This is followed by periclinal divisions throughout the primordium, with the exception of the flanking cells in some occasions, creating two cell layers (stage II; Fig. 1B). Subsequent periclinal cell divisions take place in the central zone of the primordium, producing the third cell layer (stage III) and then the fourth cell layer (stage IV; Fig.1B). Additional anticlinal cell division together with cell expansion at the innermost cell layer give rise to a dome-shaped primordium (stage V; Fig. 1B). When the cell number within the area consisting of more than one layer (MOL) (*11*) was compared at stage II - III, all TDF mutants showed an increase in a temperature dependent manner (Fig. 1, C to E). The same trend was observed in stage IV - V primordium when cell number, width of the MOL and more than three layers (MTL) (*11*) areas were quantified (Fig. 1, F to H). These results show that TDF mutants exhibit excessive cell division in the initial steps of LR development, namely as early as stage II, and indicates that the increase of cells along the lateral axis of the primordium induces the expansion of the central zone of the primordium, giving rise to an abnormally broadened and flat-shaped LR. As there were no significant increase in LR density (Fig. 1I; ANOVA, $P > 0.3$), LR fasciation in the TDF mutants seems to be the result of expansion of individual primordia, as opposed to fusion of multiple primordia due to overcrowding, observed in some other mutants (*9*, *13*).

Cloning and expression analysis of the TDF genes

To clone the TDF genes, we mapped the mutated loci in the TDF mutants based on the temperature-sensitive AR formation phenotype, which originally lead to the isolation of the mutants (fig. S1) (*16*, *17*). Candidate genes found by sequencing the mapped regions were confirmed either by a complementation test (*RRD1* and *RID4*; fig. S2) or an allelism test (*RRD2*; fig. S2). This led to the identification of *RRD1* as At3g25430, which encodes a poly(A)-specific ribonuclease (PARN)-like protein, and *RRD2* and *RID4* as At1g32415 and At2g33680, respectively, both of which encode pentatricopeptide repeat (PPR) proteins belonging to the PLS subfamily (Fig. 2A). At1g32415 has previously been reported as the responsible gene for the *cell wall maintainer 2* (*cwm2*) mutation (*21*), hence, we will refer to it as *RRD2/CWM2* from here on. *rrd1*, *rrd2*, and *rid4-1* are all nonsense mutations (Fig. 2A). The *rrd1* mutation results in an 89-amino-acid C-terminal truncation of the 618-amino-acid RRD1 protein; the mutant protein may be partially or conditionally functional. As the *rrd2* and *rid4* mutations create a stop codon close to the start codon (Fig. 2A), they are likely to eliminate gene function. Later in our study, another mutant harboring a mutation in the *RID4* gene was isolated and designated *rid4-2*. *rid4-2* exhibits LR fasciation as well as retarded seedling growth at high temperature conditions, similar to *rid4-1* (fig. S3). *rid4-2* mutation is a missense mutation, which gives rise to a single amino acid substitution (G137R) (Fig. 2A and fig. S3), presumably causing a partial reduction of gene function.

In order to elucidate the expression patterns of the TDF genes, GFP reporter studies were carried out. For *RRD1* and *RID4*, genomic constructs encompassing the promoter region to the end of the protein-coding sequence (*RRD1::RRD1:GFP, RID4::RID4:GFP*) were generated and introduced into *rrd1* and *rid4-1*, respectively. Suppression of the mutant AR phenotype demonstrated the functionality of the reporter genes (fig. S4). For both *RRD1* and *RID4*, GFP expression was largely confined to apical meristems and LR primordia in the root system (Fig. 2B, and fig. S4). This resembled the *35S::Mt-GFP* line, which express mitochondria-targeted GFP under the constitutive active cauliflower mosaic virus (CaMV) 35S promoter (Fig. 2C). At the subcellular level, fluorescence from the GFP-fusion proteins appeared punctate or granulated and largely overlapped with signals from the mitochondrion-specific dye MitoTracker Orange, demonstrating that the majority of RRD1 and RID4 proteins are localized to mitochondria (Fig. 2D). Although investigation of tissue-level *RRD2/CWM2* expression was unsuccessful due to undetectably low signals of *RRD2::RRD2:GFP*, mitochondrial localization was also confirmed for RRD2 by studying transient expression under the 35S promoter (Fig. 2E). Together, these data show that the TDF genes *RRD1*, *RRD2/CWM2*, and *RID4* encode putative RNA processing factors, all of which localize to mitochondria.

Involvement of RRD1 in poly(A) degradation of mitochondrial mRNA

PARN belongs to the DEDD superfamily of deadenylases (*22*). Human and animal studies of late have led to an increased appreciation of its participation in the maturation process of a wide variety of noncoding RNAs (*23*). In plants, however, PARN is known to have a distinct role in the removal of poly(A) tails of mitochondrial mRNA (*24*, *25*). Given the sequence similarity to PARN and its mitochondrial localization, we hypothesized that RRD1 might also be involved in regulating the poly(A) status of mitochondrial mRNA. To test this possibility, we first performed a microarray analysis of poly(A)$^+$ RNAs

prepared from wild-type and *rrd1* explants that had been induced to form LRs at 28°C, and found a substantial increase of mitochondrion-encoded poly(A)$^+$ transcripts in *rrd1* explants (Fig. 3A, and fig. S5). Since the majority of plant mitochondrial transcripts normally lack poly(A) tails, presumably due to swift removal after its addition (*26*), we suspected the possibility that the apparent sharp increase of mitochondrial transcript level might be ascribed to defective poly(A) tail removal instead of increased transcription. Indeed, comparative analysis of polyadenylated and total RNA levels by quantitative reverse transcription polymerase chain reaction (qRT-PCR) revealed a selective increase of polyadenylated transcripts (Fig. 3B). Furthermore, when the circularized RNA (CR)-RT PCR analysis (27) of *cytochrome oxidase subunit 1 (cox1)* mRNA was performed to study its 3' extremity, we found a marked increase in polyadenylated to non-polyadenylated ratio in *rrd1* compared to wild-type (Fig. 3C). In addition, the poly(A) test assay by rapid amplification of cDNA ends (RACE-PAT) (*28*) showed that polyadenylated transcript level increases at higher temperatures in *rrd1* (Fig. 3D). Taken together, these results demonstrate that RRD1 is involved in poly(A) tail removal of mitochondrial mRNAs, and that in *rrd1*, polyadenylated mitochondrial transcripts accumulate in a temperature dependent manner.

We next investigated whether the RRD1 protein itself has deadenylation activity. In previous studies, this possibility has been excluded on grounds that, in contrast to AtPARN/AHG2, RRD1 lacks three out of four amino acids essential for its function as a deadenylase (*29*). In fact, the recombinant RRD1 protein did not show any activity in conditions used for human PARN (fig. S5). We conclude that the RRD1 protein does not have deadenylase activity on its own.

To assess the effects of the observed accumulation of poly(A)+ mitochondrial transcripts in *rrd1*, we introduced the *ahg2-1* suppressor (*ags1*) mutation into *rrd1*. *ags1* is a mutation of the mitochondrion-localized poly(A) polymerase (PAP), AGS1, originally identified by its ability to counteract AtPARN/AHG2 loss of function (*24*). A substantial decrease in mitochondrial poly(A)+ transcript levels were observed in the *rrd1 ags1* double mutant compared to the *rrd1 AGS1* control (Fig. 4A). Moreover, *rrd1* phenotypes, such as temperature-dependent LR fasciation and seedling growth retardation, were significantly alleviated (Fig. 4, B and C). These results indicate that accumulation of poly(A)+ mitochondrial transcripts are the primary cause of the *rrd1* phenotype.

Involvement of RRD2 and RID4 in mitochondrial mRNA editing

PPR proteins are characterized by tandem arrays of the degenerate "PPR motif", approximately 35 amino acids in length, which enables them of recognizing specific RNA sequences through modular base-specific contacts (*30*). The PPR protein family has undergone a remarkable expansion in land plants, comprising one of largest protein families thereof (*30*). A large majority of its members are known for their participation in various aspects of organellar RNA metabolism (*19, 30*). RRD2 and RID4 belong to the PLS-class of PPR proteins, most of which have been reported as C-to-U RNA editing factors (*31*). Taking into account their localization to mitochondria (Fig. 2, D and E), we speculated the involvement of RRD2 and RID4 in RNA editing of mitochondrial transcripts. A comprehensive sequence analysis of previously reported RNA editing sites using cDNA prepared from explants induced to form LRs at 28°C revealed an almost complete abolishment of C-to-U editing at 2 sites (*cytochrome c biogenesis protein 2* (*ccb2*)-71C; *ccb3*-575C) in *rrd2* and at 6 sites (*ATP synthase subunit 4* (*atp4*)-395C, *ribosomal protein*

l5 (*rpl5)*-58C and 59C, *rps3*-1344C, *rps4*-77C and 332C) in *rid4* (Fig. 5A, fig. S7). The identification of *ccb3*-575C as a RRD2/CWM2 editing site was in agreement with the previous study of *cwm2* (*21*). RID4 editing sites showed incomplete editing in *rid4-2*, implying partial loss of function in this mutant (fig. S7). Significant identity was found among the 5' upstream sequences of editing sites affected in each mutant (fig. S8), further suggesting that RRD2 and RID4 participate in editing of these sites by means of direct contact.

In addition, all editing sites of *ccb3*, except for those that were not edited in the wild-type, showed declining levels of RNA editing in both *rrd2* and *rid4* (fig. S7). However, these sites were not considered as specific editing sites of RRD2 and RID4, since the reduced levels of editing likely reflected changes in the relative kinetics of RNA editing and transcription rather than a loss of editing activity. In support of this idea, these editing sites were incompletely edited even in the wild-type, as opposed to most other sites (fig. S7), indicating their high susceptibility to such kinetic alterations. Moreover, these sites were only partially unedited at 28°C in *rrd2* and *rid4* and showed near wild-type editing at 22°C (fig. S8). This was in contrast to the specific editing sites, which displayed absence of editing in both 22°C and 28°C conditions (fig. S8), consistent with the predicted complete lack of *RRD2/CWM* and *RID4* gene function in their respective mutants. *ccb3*_624C was also not designated a specific editing site, despite complete loss of editing in both *rrd2* and *rid4*, for it being more likely due to original lower levels of editing compared to other sites in *ccb3* (fig. S7). A lack of similarity between its upstream sequence with those of other identified editing sites reinforced this idea (fig. S8). Altogether, these results confirm the involvement of RRD2/CWM2 and RID4 in RNA editing at specific sites of mitochondrial mRNA.

Next, to investigate the effects of RRD2/CWM2 and RID4 loss of function on mitochondrial protein composition, we performed blue-native (BN)-PAGE analysis of mitochondrial extracts prepared from seed derived callus cultured for 3 days at 22°C or 28°C after a 19-day 22°C incubation period. This revealed a substantial loss of complex V (ATP synthase complex) in *rid4* at both 22°C and 28°C culture conditions (Fig. 5B), likely caused by defective mRNA editing of *atp4* (Fig. 5A), a component of this protein complex. Noticeable differences were not found in *rrd1* and *rrd2*. As *ccb2* and *ccb3*, the two mitochondrial genes targeted by RRD2/CWM2, are related to cytochrome c (cyt c) maturation (*32*), we quantified cyt c levels in *rrd2*. Cyt c levels on a per mitochondria basis were found to be decreased in *rrd2* callus cultured at 28°C for 3 days (Fig. 5, C and D) in two out of three cultures, although the difference was not statistically significant when all three results were included. This decrease of cyt c levels in *rrd2* was in concordance with previous analysis of *cwm2* (21). At 22°C, however, no significant difference was observed between *rrd2* and the wild type. Furthermore, we found that the difference in cyt c levels was more pronounced after longer periods of culture at 28°C (Fig. 5, E and F). These results indicate that in *rrd2*, cyt c maturation activity was affected to a greater extent at higher temperatures, at least in callus, which possesses root-tissue like properties, possibly explaining the temperature-dependent nature of its phenotype. The data above demonstrate that in both *rrd2* and *rid4*, production of certain components of the mitochondrial electron transport chain is hampered as a result of defective mRNA editing.

Effects of defective mitochondrial respiration on LR formation

Based on the results of *rrd2* and *rid4*, we speculated that there might be a relationship between mitochondrial electron transport and cell division control during LR morphogenesis. Indeed, when LRs were induced from wild-type in the presence of rotenone (complex I inhibitor), antimycin A (complex III inhibitor), or oligomycin (complex V inhibitor), LR fasciation was observed, providing evidence that electron transport chain defects are the underlying cause of the TDF LR phenotype (Fig. 6, A to D). To further investigate the underlying molecular pathway, we next asked whether either reduced ATP synthesis, or reactive oxygen species (ROS) generation, phenomena commonly associated with defective mitochondrial respiration might be involved. We found that the respiratory uncoupler carbonylcyanide m-chlorophenyl-hydrazone (CCCP) did not have any increasing effect on LR width (Fig. 6E), although LR growth inhibition was observed in a dose dependent manner (Fig. 6F), whereas the ROS inducer paraquat (PQ) gave rise to significant fasciation of LRs (Fig. 6, G and H). Furthermore, application of ROS scavenger ascorbate resulted in a reversal of LR broadening by PQ treatment (Fig. 6, G and H). The same effect was observed against the *rid4-2* mutation as well. These data suggest that the increase in the levels of ROS but not the decrease in the levels of ATP acts downstream of defective mitochondrial respiration to promote excessive cell division during LR development in the TDF mutants.

Local gradient formation of auxin is important for LR initiation and the subsequent organization of the LR primordium (*5*-*7*). Strong genetic perturbations of polar auxin transport result in homogenous proliferation of the pericycle cell layer in large regions of the root upon exogenous auxin treatment. In addition, chemical inhibition of auxin polar transport by naphthylphthalamic acid (NPA) gives rise to broadened LR primordia similar to fasciated LRs of the TDF mutants (fig. S9). These data indicate a role for local auxin gradient formation in restricting proliferative capacity during LR formation, which is required for proper LR morphogenesis. Since recent studies have suggested an antagonistic relationship between mitochondrion-generated ROS and auxin signaling (*40*), we tested whether LR fasciation due to ROS generation is mediated by altered accumulation of auxin in early LR primordia. When the expression pattern of the auxin-responsive β-glucuronidase marker *DR5::GUS* (*5*-*7*) was examined at early stages of LR induction, however, no difference between control and PQ treated root segments were observed, whereas treatment with NPA resulted in enhanced expression along the entire root segment (Fig. 6I). This result indicates that ROS-induced LR fasciation is not caused by an impairment in auxin gradient formation.

Discussion

LR fasciation resulting from excessive cell division during early LR development

In the present study, we investigated fasciated LR formation observed at high-temperature conditions in the TDF mutants utilizing the semi-synchronous LR induction system (*20*). By measurement of cell number and primordium width, we found that fasciation of LRs is caused by excessive anticlinal cell division that takes place as early as stage II of LR development (Fig. 1). The lack of increase in LR density (Fig. 1I) suggested that LR fasciation is due to expansion of individual primordia, rather than fusion of multiple primordia, which is the case in some other mutants that form abnormally broadened

LRs (*9*, *13*). The data are in agreement with the previous result of the temperature shift experiment, which demonstrated that the first 48 h period following LR induction is critical for LR fasciation in the TDF mutants (*18*), since stage II to early stage III primordia are formed within this time frame (Fig. 2D) (*20*). The previous characterization of the TDF mutants also showed that fasciated LR primordia exhibit specific enlargement of inner root tissue marked by the expression of *SHORT ROOT* (*SHR*), while the number of cell layers outside the SHR-expressing layer are normal (*18*). A recent study revealed that the area of SHR expression is first established during stage II, where it is confined to the inner layer of the two-cell layered primordium (*4*). In subsequent stages, SHR is expressed in cell files derived from the inner layer, which develop into the stele of the LR (*4*). In light of the above-mentioned data, it is plausible that during LR fasciation in the TDF mutants, differentiation mechanisms of the tissue layers at stage II are more or less intact, and that the increased number of cells of stage II primordia consequently leads to the expansion of the SHR expression in the inner cell layer. Taken together, these data indicate that the TDF mutants are impaired in the restriction of the number of anticlinal cell divisions at early stages of LR development, which leads to LR fasciation.

Identification of RRD1 as a PARN-like protein involved in poly(A) tail removal of mitochondrial mRNA

PARN is a 3' exoribonuclease of the DEDD superfamily (*22*), which shows a strong preference for adenine as a substrate (*22*, *23*). In plants, PARN is known to be involved in the removal of poly(A) tails of mitochondrial transcripts (*24*, *25*). In this study, we identified *RRD1* as a gene encoding a PARN-like protein (Fig. 2A). Analysis of the *RRD1::RRD1:GFP* line revealed strong expression in primordial cells during LR development, in addition to weak expression in surrounding tissue (Fig. 2B). This likely reflects the distribution of mitochondria, since a similar expression pattern is observed in the mitochondrion-targeted GFP line harboring *35S::Mt-GFP* (Fig. 2C). Further analysis of *rrd1* demonstrated the participation of RRD1 in poly(A) tail degradation of mitochondrial mRNA. First, a microarray analysis revealed a global increase of poly(A)+ mitochondrial transcript levels in *rrd1* (Fig. 3A). Next, qRT-PCR of several genes confirmed that in *rrd1*, polyadenylated mitochondrial mRNA levels are substantially increased whereas total (polyadenylated + nonpolyadenylated) mRNA levels are not significantly altered (Fig. 3B). Finally, CR-RT PCR analysis of *cox1* mRNA showed that, as was the case reported for the loss of function mutant of AtPARN/AHG2, mitochondrial mRNAs with polyadenylation at the 3' ends were much more abundant in *rrd1* (Fig. 3C) compared to the wild type, in which only a very small fraction of mitochondrial mRNAs are polyadenylated (Fig. 3C) (*24*, *26*).

In plant mitochondria, immature 3' extremities of mRNA, along with irregular RNAs, such as 3' misprocessed mRNAs, rRNA maturation byproducts, and cryptic transcripts, are known to be polyadenylated before they are degraded by mitochondrial polynucleotide phosphorylase (mtPNPase) (*26*). Indeed, down-regulation of mtPNPase in *Arabidopsis* results in accumulation of long preprocessed mRNA, as well as irregular RNA, the majority of which are polyadenylated (*26*). In *rrd1*, lengthy preprocessed mRNAs do not seem to be accumulated, since the size of RACE-PAT assay products correspond to that of previously reported mature transcript ends (Fig. 3D). Although whether byproduct accumulation takes place is not clear, given the absence in *ahg2* (*24*), it might be unlikely. Furthermore, total mitochondrial mRNA levels are unchanged as mentioned above (Fig. 3B), suggesting that RRD1

is not involved in controlling mRNA abundance by promoting degradation. Taking these considerations into account, RRD1 has a distinct role to mtPNPase, and seems to be specifically involved in 3' processing of near-matured mRNA. Further testing will be needed to address the physiological relevance of such 3' processing in mitochondrial RNA function.

The mode of action of the RRD1 protein remains unclear. The absence of the three out of four catalytic amino acids (DEDD) essential for ribonuclease activity (fig. S6) (*29*), together with the apparent lack of deadenylase activity of the recombinant RRD1 protein (fig. S5, D and E) indicated that RRD1 requires additional factors for its participation in poly(A) tail removal.

Nonetheless, deficient removal of poly(A) tails from mitochondrial transcripts seems to be primary cause of the *rrd1* phenotype. This is evidenced by the fact that introduction of a mutation of the mitochondria-localized poly(A) polymerase gene *AGS1* into *rrd1*, substantially alleviated both the accumulation of poly(A)+ mitochondria transcripts (Fig. 4A) and various aspects of the *rrd1* phenotype, including LR fasciation (Fig. 4, B and C). As most protein coding genes in the *Arabidopsis* mitochondrial genome are involved in the biogenesis of the electron transport chain (*19*), it is likely that mitochondria of *rrd1* carry defects in respiratory activity. However, the exact impact of altered poly(A) status of mRNAs in mitochondria to electron transport in *rrd1* remains unclear. In fact, unlike the AtPARN/AHG2 loss of function mutant *ahg2*, which shows a reduction in complex III levels (*24*), no significant difference of respiratory chain composition has been detected in *rrd1* so far (Fig. 5B).

Identification of RRD2 and RID4 as PLS-class PPR proteins involved in mitochondrial mRNA editing

PPR proteins are known for their role in regulating various aspects of organellar post-transcriptional gene expression, such as RNA stabilization, RNA cleavage, RNA splicing, RNA editing, and translation (*19*, *30*). They are characterized by the tandem assembly of degenerate protein motifs, of about 35 amino acids in length, termed PPR motifs (*30*). The PPR motifs allow PPR proteins to recognize specific sites of single-stranded RNA through a one-motif to one-base interaction (*30*). The PLS-class PPR proteins contain three types of PPR motifs, the P motif (normally 35 a. a.), L motif (long; 35 - 36 a. a.) and the S motif (short; 31 a. a.), in contrast to the P-class PPR proteins, which only contain P motifs (*30*, *33*). Our study identified *RRD2* and *RID4* as At1g32415 and At2g33680, respectively, both of which encode PPR proteins belonging to the PLS subclass (Fig. 2A). At1g32415 had previously been reported as the gene responsible for the *cwm2* mutant (*21*). A predominant role for PLS-class PPR proteins in RNA editing has been demonstrated with more than 50 out of a total of approximately 200 in Arabidopsis identified as C-to-U editing factors of mitochondria or plastid RNA (*31*). By analysis of GFP-fusion proteins, both RRD2 and RID4 were shown to localize mainly to mitochondria (Fig. 2, D and E). The expression pattern of *RID4::RID4:GFP* in the root resembled the distribution of Mt-GFP, thus likely reflecting mitochondrial abundance (Fig. 2, B and C). Moreover, a comprehensive analysis of mitochondrial RNA editing revealed abolishment of editing at specific sites in *rrd2* and *rid4* (Fig. 5A and fig. S7). We conclude that both RRD2/CWM2 and RID4 are PLS-class PPR proteins involved in mitochondrial mRNA editing.

In *rrd2,* editing at 71C of *ccb2* and 575C of *ccb3* was found to be absent (Fig. 5A). Both *ccb2* (also known as *ccb206*, *ccmB*, *ABCI2*, and *AtMg00110*) and *ccb3* (also known as *ccb256*, *ccmC*, *ABCI3*, and *AtMg00900*) encode multisubunit ATP-binding cassette (ABC) proteins, involved in the maturation of mono hemic c-type cytochromes, the soluble cytochrome c, and the membrane-bound cyt c_1 of complex III (*32*). Of the two editing sites, *ccb3*-575C had previously been reported as a target of *RRD2/CWM2* (*21*), whereas *ccb2*-71C is a newly discovered target. A decrease in the level of cytochrome c was detected in *rrd2*, which is consistent with the previous report for *cwm2* (*21*). The data demonstrate the role of *RRD2/CWM2* in cytochrome c maturation via RNA editing of cytochrome c biogenesis factors.

In *rid4*, striking reductions of RNA editing at *atp4*-395C, *rpl5*-58 and 59C, *rps3*-1344C, *rps4*-77C, and *rps4*-332C were observed. *atp4* (also known as *orf25*, *AtMg00640*) encodes the peripheral stalk protein (subunit b) of the mitochondrial ATP synthase complex (complex V) (*34*). *rpl5*, *rps3*, and *rps4* encode mitochondrial ribosome proteins. Analysis of mitochondrial protein complexes showed a dramatic decrease in the level of complex V in *rid4*, probably due to impaired editing of *atp4*-395C. This is similar to the *organelle transcript processing 87* (*otp87*) mutant of Arabidopsis, in which editing of *atp1*-1178C is deficient (*35*). These data show that the formation of complex V could be disrupted by defective RNA editing of a single subunit gene. Considering that the C-to-U editing of the *rps4* transcript at a different site (*rps4*-377) has been shown to affect mitochondrial ribosome assembly (*36*), it is possible that the *rid4* mutation also has some impact on the mitochondrial ribosome.

Recent advancement in our mechanistic understanding of RNA binding by PLS-class PPR proteins has led to the identification of residues at certain positions within the PPR motifs important for ribonucleotide recognition (*30*, *31*). By mapping these residues of previously reported RNA editing PPR proteins to their binding sites that are located 5' upstream of the editing sites, the so-called 'PPR code' has been elucidated, which enables the matching of PPR proteins to their candidate editing targets, and vice versa (*31*). According to the recently refined PPR code prediction (*31*), RID4 highly ranked as a potential binding protein of *atp4*-395C (18^{th}, $P = 4.35 \times 10^{-2}$), *rpl5*-58C (5^{th}, $P = 3.04 \times 10^{-2}$) and *rps4*-332C (2^{nd}, $P = 4.06 \times 10^{-3}$). Conversely, these sites were among the predicted editing sites of RID4 ($P < 0.05$) (*31*). With regard to RRD2, however, the newly identified binding site (*ccb2*-71C) ranked very low, despite the incorporation of RRD2/CWM2 binding to *ccb3*-575C as learning data for the PPR code prediction (*31*). This disagreement may be related to the unusual arrangement of PPR motifs in RRD2 where repeats of SS motifs are prevalent, in contrast to canonical PLS-class PPRs, such as RID4, which follow the $(P1\text{-}L1\text{-}S1)_n$-P2-L2-S2 pattern (Fig. 2A) (*33*). Nevertheless, given the similarity between the upstream sequences of editing sites which are severely affected by *rrd2* and *rid4* (fig. S8), they are likely edited by RRD2 and RID4 via direct interaction. The presented data will contribute to the further improvement of PPR protein target estimation.

Temperature-sensitivity of the TDF mutants

A distinct feature of the TDF LR phenotype is that it is observed exclusively at high temperature conditions (*16-18*). Our study revealed some differences in the origin of temperature-sensitiveness among the TDF mutants. The *rrd1* mutation causes a truncation of the C-terminal domain of the RRD1 protein (Fig. 2A). This finding, together with the enhancement of poly(A)+ mitochondrial mRNA

accumulation at elevated temperatures (Fig. 3D) implies that in *rrd1,* RRD1 is partially functional at least at the permissive temperature and that its activity is more severely affected at the non-permissive temperature. In contrast, the *rrd2* and *rid4-1* mutations introduce a stop codon close to the N-terminus of RRD2 and RID4, respectively, likely resulting in the total loss of their functions (Fig. 2A). The complete abolishment of RNA editing of RRD2 and RID4 target sites in the *rrd2* and *rid4-1* mutants regardless of temperature (Fig. 5A and fig. S8) further supported this idea. However, in *rrd2*, deficient cytochrome C biogenesis was observed only at high temperature (Fig. 5, C and D). This might be accounted for by the possible temperature-sensitiveness of the function of either *ccb2* or *ccb3*, that are altered in amino acid sequence in *rrd2*, due to impaired RNA editing (Fig. 5A). In *rid4-1*, a huge reduction in complex V biosynthesis was observed both at permissive and non-permissive temperatures (Fig. 5B). From these results, a possible explanation for the temperature-sensitivity of the LR fasciation phenotype of *rid4-1* is that complex V deficiency might be more deleterious at higher temperatures (*17*).

Impairment of mitochondrial electron transport as the primary cause of LR fasciation

Phenocopy of the LR fasciation phenotype of the TDF mutants by treatment with respiratory inhibitors demonstrated the causal relationship between defective mitochondrial electron transport and excessive cell division during early LR development (Fig. 6, A to D). Mitochondrial electron transport is best known for its role in driving ATP synthesis through oxidative phosphorylation. Given the lack of LR fasciation when treated with mitochondrial uncoupler CCCP (Fig. 6, E and F), reduced ATP production seems unlikely to be the cause of LR fasciation. The fact that the huge reduction of complex V levels in *rid4* (Fig. 5B) does not lead to LR fasciation at permissive temperature (*18*), is also supportive of this idea. Experiments using the ROS inducer PQ and the antioxidant ascorbate (Fig. 6, G and H), pointed to mitochondria ROS generation as the potential trigger of LR fasciation. A previous study has also observed enhanced cell division by application of another ROS inducer alloxan, during auxin-induced LR formation (*37*). In agreement with this 'ROS hypothesis', all three respiratory inhibitors used in our study (rotenone, antimycin A, oligomycin) are known as potent inducers of oxidative stress (*38*).

ROS has been implicated in stress-induced morphogenic responses (SIMR) (*39*). Several studies have shown the involvement of plant hormonal regulation in ROS-triggered SIMR. Altered auxin levels and/or distribution has been proposed as a potential mediator in modulating cell proliferation in response to oxidative stress (*38*, *39*). Several recent studies have found antagonistic interactions between auxin signaling and ROS (*40*). Auxin is a critical factor in LR development and the centripetal auxin gradient formation in early stage LR primordia is thought to contribute to the organization of the LR primordium (*6*, *7*). However, neither the pattern nor intensity of auxin response visualized by the *DR5::GUS* reporter seemed to be altered under PQ treatment, in contrast to the diffuse pattern observed when the auxin polar transport inhibitor NPA was applied (Fig. 6I). This indicates that ROS-induced LR fasciation is not attributable to the failure in auxin gradient formation. Further studies of LR fasciation caused by oxidative stress will likely uncover novel aspects of cell proliferation control during plant organogenesis.

Material and methods

Plant materials and growth condition

Arabidopsis thaliana (L.) Heynh. ecotypes Columbia (Col) and Landsberg *erecta* (L*er*) were used in this work. The TDF mutants *rrd1*, *rrd2*, and *rid4-1* were described previously (*16-18*). The *ags1* mutant (*ags1-1*) was also described previously (*24*). *35S::Mt-GFP* was a gift from W. Sakamoto. *rid4-2* was derived from an ethyl methanesulfonate-mutagenized population of the L*er* strain of *Arabidopsis thaliana*. SALK_027874 was obtained from the Arabidopsis Biological Resource Center. *rrd1* mutant strains harboring either *ags1* or *AGS1*^{c} were obtained by *rrd1* (Ler background) × *ags1* (Col background) and *rrd1* ×Col crosses, respectively.

Seedlings were aseptically grown on Murashige–Skoog medium supplemented with 1.0% (w/v) sucrose, buffered to pH 5.7 with 0.05% (w/v) 2-morpholinoethanesulfonic acid (MES), and solidified with 1.5% (w/v) agar under continuous light (10–15 μmol m^{-2} s^{-1}) at 22°C. For self-propagation and crossing, plants were grown on vermiculite under continuous light (approximately 50 μmol m^{-2} s^{-1}) at 22°C unless otherwise indicated.

LR induction

As described previously (*20*), explants were prepared from 4-day-old seedlings, and cultured on root-inducing medium (RIM) under continuous light (15–25 μmol m^{-2} s^{-1}) for the induction of semi-synchronous formation of LRs. RIM was B5 medium supplemented with 2.0% (w/v) glucose and 0.5 mg l^{-1} indole-3-butyric acid, buffered to pH 5.7 with 0.05% (w/v) MES, and solidified with 0.25% (w/v) gellan gum. Culture temperature was set to 22°C for the permissive condition and to 28°C for the non-permissive condition.

Histological analysis

For whole-mount observation, tissue samples were fixed in 25 mM sodium phosphate buffer (pH 7.0) containing 2% (w/v) formaldehyde and 1% (w/v) glutaraldehyde, rinsed with 100 mM sodium phosphate buffer (pH 7.0), and cleared with an 8:1:2 (w/v/v) mixture of chloral hydrate, glycerin, and water. Observations were made with a microscope equipped with Nomarski optics (BX50-DIC; Olympus) to obtain differential interference contrast (DIC) images.

For morphometric analysis of LR primordia, in order to highlight cell organization, the method of ref. 1 was instead employed for tissue fixation and clearing. Developmental stages of LR primordia were determined according to ref. 1. LR primordia at Stages II to early III and at Stages IV to V were chosen from samples that had been collected after 16 to 24 hours and 24 to 48 hours of culture in the semi-synchronous root induction system, respectively, and were measured for their width and cell number.

For histochemical detection of GUS reporter expression, tissue samples were fixed in 90% (v/v) acetone overnight at −20˚C, rinsed with 100 mM sodium phosphate (pH 7.0), and incubated in X-Gluc solution [0.5 mg ml^{-1} 5-bromo-4-chloro-3-indolyl b-D-glucuronide cyclohexylammonium salt, 0.5 mM potassium ferricyanide, 0.5 mM potassium ferrocyanide, 100 mM sodium phosphate (pH 7.4)] for 140 min at 37 ˚C. After rinsing with 100 mM sodium phosphate buffer (pH 7.0), the samples were mounted

on glass slides with an 8:1:2 (w/v/v) mixture of chloral hydrate, glycerin, and water, and then subjected to DIC microscopy.

Chromosome mapping

The TDF mutants in the L*er* background were crossed with the wild-type Columbia (Col) strain, and the resultant F_1 plants were self-pollinated to produce F_2 seeds or test-crossed with the mutant plants to produce TC_1 seeds. The TC_2 lines were then developed by separately collecting self-pollinated progenies from each individual TC_1 plant. F_2 plant or TC_2 lines were checked for the ability of adventitious root formation at 28°C and for DNA polymorphism between L*er* and Col. Chromosome locations of the TDF mutations were determined on the basis of linkage between the mutations and the L*er* alleles of polymorphic marker loci.

Identification of the TDF genes

Sequencing of the genomic regions to which the TDF mutations were mapped led to identification of candidates of *RRD1*, *RRD2*, and *RID4* as At3g25430, At1g32415, and At2g33680, respectively. Identification of these genes was confirmed by the complementation test or the allelism test as described below.

For the complementation test, genomic clones GL07, encompassing At3g25430 (2.9-kbp 5´-flanking sequence, 2.6-kbp coding sequence, and 2.5-kbp 3´-flanking sequence), and GL91321, encompassing At2g33680 (1.8-kbp 5´-flanking sequence, 3.5-kbp coding sequence, and 2.0-kbp 3´-flanking sequence), were isolated from a transformation-competent genome library[26], and introduced into the *rrd1* and *rid4* mutants, respectively. The resultant transformants were examined for the ability of adventitious root formation at 28˚C. To determine allelism between *rrd2* and SALK_027874, which carries a T-DNA insertion in At1g32415, F_1 progeny derived by crossing *rrd2* with SALK_027874 was examined for the ability of adventitious root formation at 28˚C.

Plasmid construction

Genomic DNA from L*er* was used as a template for PCR-based amplification of DNA fragments of interest. *RRD1::RRD1:GFP* was constructed by inserting the –2780/+2495 region of the *RRD1* gene (+1 = the first base of the translation initiation codon), which encompassed the genomic region from the promoter to the end of the protein-coding sequence, and the coding sequence of sGFP into pGreen0029 (John Innes Centre). *RID4::RID4:GFP* was similarly constructed by inserting the –2297/+2181 region of the *RID4* gene and the sGFP-coding sequence into pGreen0029. For the construction of *35S::RRD2:GFP,* the +1/+2283 region of the *RRD2* gene was inserted into the pSHO1 vector. Plasmids for the PARN activity assay was constructed by inserting the sequence of RRD1 or hPARN sequence into the pHAT vector. 24 amino acids of the C-terminal of RRD1 was deleted. The SEP-tag C9D was added to the C-terminal of both RRD1 and hPARN sequences.

Plant transformation

DNAs such as reporter gene constructs and genomic fragments were transformed into *Agrobacterium tumefaciens* and then into *A. thaliana* by the floral dip method or its modified version . Transgenic plants were selected by antibiotic resistance and genotyped by PCR for the introduction of the correct transgene.

Expression and localization analysis of GFP reporters

Expression patterns of *RRD1* and *RID4* were examined with transgenic plants harboring *RRD1::RRD1:GFP* and *RID4::RID4:GFP*, respectively. Roots of 6-day-old seedlings of these plants were counterstained with 10 mg l^{-1} of propidium iodide and fluorescence images were obtained using a confocal microscope (FV3000; Olympus). Expression analysis of 35S::Mt-GFP was performed in the same conditions using a different confocal microscope (FV1200; Olympus).To investigate subcellular localization of the RRD1 and RID4 proteins, protoplasts were prepared from calli that had been induced from the *RRD1::RRD1:GFP* and *RID4::RID4:GFP* explants. The protoplasts were incubated with 100 nM Mitotracker Orange (Invitrogen) for 15 minutes to visualize mitochondria and then observed using the LSM710 system (Carl Zeiss).

Microarray analysis and data processing

For microarray analysis, total RNA was extracted with TRIzol reagent (Invitrogen) from explants that had been cultured on RIM for 12 hours in the semi-synchronous lateral root induction system and purified using the RNeasy microkit (QIAGEN). Affymetrix ATH1 microarrays were hybridized with biotinylated cRNA targets prepared from the RNA samples according to the manufacturer's instructions. It should be noted here that all the targets were derived from poly(A)$^+$ RNA in principal because the T7-oligo(dT)$_{24}$ primer was used for reverse-transcription at the first step of target preparation. The data sets obtained were processed with a variant of MAS5.0 utilizing robust radius-minimax estimators. Experiments were performed in biological triplicates. The details of the microarray data have been deposited in the Gene Expression Omnibus (http://www.ncbi.nlm.nih.gov/geo/) under accession number GSE34595.

Analysis of mRNA polyadenylation status with poly(A) test assay

Poly(A) test assay was performed principally according to (*28*). Total RNA was extracted with TRIzol reagent (Invitrogen) from explants that had been cultured on RIM for 12 hours in the semi-synchronous lateral root induction system. To eliminate genomic DNA, 500 ng of total RNA was treated with RNase-free DNase I (Promega), and reverse-transcribed with T7-oligo(dT)$_{24}$ as a primer using the PrimeScript II 1st strand cDNA Synthesis kit (TaKaRa). Then the poly(A) tail status was analyzed by PCR with a combination of gene-specific and T7 promoter primers. The thermal cycling program consisted of initial 2-minute denaturation at 95°C followed by 30 cycles of 20 seconds at 95°C, 20 seconds at 57°C, and 10 seconds at 72°C. Primers for the poly(A) test assay are listed in Supplementary table 1.

qRT-PCR analysis

For qRT-PCR, total RNA was extracted with TRIzol reagent (Invitrogen) from explants that had been cultured for 12 hours in the semi-synchronous root induction system. To eliminate genomic DNA, 500 ng of total RNA was treated with RNase-free DNase I (Promega), and reverse-transcribed with a random hexamer or oligo$(dT)_{24}$ primer using SYBR Premix ExTaq II (TaKaRa). qRT-PCR reactions were performed with gene-specific forward and reverse primers using the PrimeScript RT-PCR kit (TaKaRa) on the StepOne® Real-Time PCR system (Applied Biosystems). The thermal cycling program consisted of initial 30-second denaturation at 95°C followed by 40 cycles of 5 seconds at 95°C and 30 seconds at 60°C. At the end of run, melting curves were established for each PCR product to check the specificity of amplification. Expression levels of mRNAs of interest were normalized relative to *TUBULIN4* (At5g44340) expression. DNA fragments amplified from poly$(A)^+$ transcripts of several genes including *cob* were sequenced to check the occurrence of mitochondrial editing, which confirmed that they are derived from the mitochondrial genome no but from their copies present in chromosome 2. Experiments were performed in biological triplicates. Primers for the qRT-PCR analysis are listed in Supplementary table 1.

Rererences

1. L. Taiz, E. Zeiger, I. M. Møller, and A. Murphy, “Plant physiology and development” (Sinauer Associates, ed. 6, Cary, NC, USA, 2014)

2. H. H. Torres-Martinez, G. Rodriguez-Alonso, S. Shishkova, and J. G. Dubrovsky, “Lateral root primordium morphogenesis in angiosperms,” Frontiers in Plant Science, vol. 10, Mar, 2019.

3. D. von Wangenheim, J. Fangerau, A. Schmitz, R. S. Smith, H. Leitte, E. H. K. Stelzer, and A. Maizel, “Rules and self-organizing properties of post-embryonic plant organ cell division patterns,” Current Biology, vol. 26, no. 4, pp. 439-449, Feb, 2016.

4. T. Goh, K. Toyokura, D. M. Wells, K. Swarup, M. Yamamoto, T. Mimura, D. Weijers, H. Fukaki, L. Laplaze, M. J. Bennett, and S. Guyomarc'h, “Quiescent center initiation in the Arabidopsis lateral root primordia is dependent on the SCARECROW transcription factor,” Development, vol. 143, no. 18, pp. 3363-3371, Sep, 2016.

5. J. Lavenus, T. Goh, I. Roberts, S. Guyomarc'h, M. Lucas, I. De Smet, H. Fukaki, T. Beeckman, M. Bennett, and L. Laplaze, “Lateral root development in Arabidopsis: fifty shades of auxin,” Trends in Plant Science, vol. 18, no. 8, pp. 455-463, Aug, 2013.

6. E. Benková, M. Michniewicz, M. Sauer, T. Teichmann, D. Seifertová, G. Jürgens, and J. Friml, “Local, efflux-dependent auxin gradients as a common module for plant organ formation,” Cell, vol. 115, no. 5, pp. 591-602, Nov, 2003.

7. N. Geldner, S. Richter, A. Vieten, S. Marquardt, R. A. Torres-Ruiz, U. Mayer, and G. Jürgens, “Partial loss-of-function alleles reveal a role for GNOM in auxin transport-related, post-embryonic development of Arabidopsis,” Development, vol. 131, no. 2, pp. 389-400, Jan, 2004.

8. I. De Smet, S. Lau, U. Voß, S. Vanneste, R. Benjamins, E. H. Rademacher, A. Schlereth, B. De Rybel, V. Vassileva, W. Grunewald, M. Naudts, M. P. Levesque, J. S. Ehrismann, D. Inzé, C. Luschnig, P. N. Benfey, D. Weijers, M. C. E. Van Montzxagu, M. J. Bennett, G. Jürgens, and T. Beeckman, “Bimodular auxin response controls organogenesis in Arabidopsis,” Proceedings of the National Academy of Sciences of the United States of America, vol. 107, no. 6, pp. 2705-2710, Feb, 2010.

9. I. De Smet, V. Vassileva, B. De Rybel, M. P. Levesque, W. Grunewald, D. Van Damme, G. Van Noorden, M. Naudts, G. Van Isterdael, R. De Clercq, J. Y. Wang, N. Meuli, S. Vanneste, J. Friml, P. Hilson, G. Jürgens, G. C. Ingram, D. Inzé, P. N. Benfey, and T. Beeckman, “Receptor-like kinase ACR4 restricts formative cell divisions in the Arabidopsis root,” Science, vol. 322, no. 5901, pp. 594-597, Oct, 2008.

10. E. Murphy, L. D. Vu, L. Van den Broeck, Z. F. Lin, P. Ramakrishna, B. van de Cotte, A. Gaudinier, T. Goh, D. Slane, T. Beeckman, D. Inze, S. M. Brady, H. Fukaki, and I. De Smet, “RALFL34 regulates formative cell divisions in Arabidopsis pericycle during lateral root initiation,” Journal of Experimental Botany, vol. 67, no. 16, pp. 4863-4875, Aug, 2016.

11. A. Hirota, T. Kato, H. Fukaki, M. Aida, and M. Tasaka, “The auxin-regulated AP2/EREBP gene PUCHI is required for morphogenesis in the early lateral root primordium of Arabidopsis,” Plant Cell, vol. 19, no. 7, pp. 2156-2168, Jul, 2007.

12. Y. J. Du, and B. Scheres, “PLETHORA transcription factors orchestrate de novo organ patterning during Arabidopsis lateral root outgrowth,” Proceedings of the National Academy of Sciences of the United States of America, vol. 114, no. 44, pp. 11709-11714, Oct, 2017.

13. Y. Benitez-Alfonso, C. Faulkner, A. Pendle, S. Miyashima, Y. Helariutta, and A. Maule, “Symplastic intercellular connectivity regulates lateral root patterning,” Developmental Cell, vol. 26, no. 2, pp. 136-147, Jul, 2013.

14. S. Napsucialy-Mendivil, R. Alvarez-Venegas, S. Shishkova, and J. G. Dubrovsky, “ARABIDOPSIS HOMOLOG of TRITHORAX1 (ATX1) is required for cell production, patterning, and morphogenesis in root development,” Journal of Experimental Botany, vol. 65, no. 22, pp. 6373-6384, Dec, 2014.

15. J. E. M. Vermeer, D. von Wangenheim, M. Barberon, Y. Lee, E. H. K. Stelzer, A. Maizel, and N. Geldner, “A spatial accommodation by neighboring cells is required for organ initiation in Arabidopsis,” Science, vol. 343, no. 6167, pp. 178-183, Jan, 2014.

16. M. Sugiyama, “Isolation and initial characterization of temperature-sensitive mutants of *Arabidopsis thaliana* that are impaired in root redifferentiation,” Plant and Cell Physiology, vol. 44, no. 6, pp. 588-596, Jun, 2003.

17. M. Konishi, and M. Sugiyama, “Genetic analysis of adventitious root formation with a novel series of temperature-sensitive mutants of *Arabidopsis thaliana*,” Development, vol. 130, no. 23, pp. 5637-5647, Dec, 2003.

18. K. Otsuka, and M. Sugiyama, “Tissue organization of fasciated lateral roots of Arabidopsis mutants suggestive of the robust nature of outer layer patterning,” Journal of Plant Research, vol. 125, no. 4, pp. 547-554, Jul, 2012.

19. K. Hammani, and P. Giege, “RNA metabolism in plant mitochondria,” Trends in Plant Science, vol. 19, no. 6, pp. 380-389, Jun, 2014.

20. M. Ohtani, T. Demura, and M. Sugiyama, “Particular significance of SRD2-dependent snRNA accumulation in polarized pattern generation during lateral root development of Arabidopsis,” *Plant and Cell Physiology,* vol. 51, no. 12, pp. 2002-2012, Dec, 2010.

21. Z. B. Hu, R. Vanderhaeghen, T. Cools, Y. Wang, I. De Clercq, O. Leroux, L. Nguyen, K. Belt, A. H. Millar, D. Audenaert, P. Hilson, I. Small, G. Mouille, S. Vernhettes, F. Van Breusegem, J. Whelan, H. Hofte, and L. De Veylder, “Mitochondrial defects confer tolerance against cellulose deficiency,” The Plant Cell, vol. 28, no. 9, pp. 2276-2290, Sep, 2016.

22. A. Pavlopoulou, D. Vlachakis, N. A. A. Balatsos, and S. Kossida, “A comprehensive phylogenetic analysis of deadenylases,” *Evolutionary Bioinformatics,* vol. 9, pp. 491-497, 2013.

23. D. Lee, D. Park, J. H. Park, J. H. Kim, and C. Shin, “Poly(A)-specific ribonuclease sculpts the 3' ends of microRNAs,” *RNA,* vol. 25, no. 3, pp. 388-405, Mar, 2019.

24. T. Hirayama, T. Matsuura, S. Ushiyama, M. Narusaka, Y. Kurihara, M. Yasuda, M. Ohtani, M. Seki, T. Demura, H. Nakashita, Y. Narusaka, and S. Hayashi, “A poly(A)-specific ribonuclease directly regulates the poly(A) status of mitochondrial mRNA in Arabidopsis,” *Nature Communications,* vol. 4, Aug, 2013.

25. Kanazawa, Y. Ikeda, R. Nishihama, S. Yamaoka, N. H. Lee, K. T. Yamato, T. Kohchi, and T. Hirayama, “Regulation of the poly(A) status of mitochondrial mRNA by poly(A)-specific ribonuclease is conserved among land plants,” *Plant and Cell Physiology,* vol. 61, no. 3, pp. 470-480, Mar, 2020.

26. S. Holec, H. Lange, J. Canaday, and D. Gagliardi, “Coping with cryptic and defective transcripts in plant mitochondria,” Biochimica et biophysica acta, vol. 1779, no. 9, pp. 566-73, 2008-Sep, 2008.

27. J. Forner, B. Weber, S. Thuss, S. Wildum, and S. Binder, “Mapping of mitochondrial mRNA termini in *Arabidopsis thaliana*: t-elements contribute to 5 ' and 3 ' end formation,” *Nucleic Acids Research,* vol. 35, no. 11, pp. 3676-3692, Jun, 2007.

28. F. J. Salles, W. G. Richards, and S. Strickland, “Assaying the polyadenylation state of mRNAs,” *Methods-a Companion to Methods in Enzymology,* vol. 17, no. 1, pp. 38-45, Jan, 1999.

29. S. V. Reverdatto, J. A. Dutko, J. A. Chekanova, D. A. Hamilton, and D. A. Belostotsky, “mRNA deadenylation by PARN is essential for embryogenesis in higher plants,” *RNA,* vol. 10, no. 8, pp. 1200-1214, Aug, 2004.

30. A. Barkan, and I. Small, “Pentatricopeptide repeat proteins in plants,” Annual Review of Plant Biology, Vol 65, vol. 65, pp. 415-42, 2014.

31. T. Kobayashi, Y. Yagi, and T. Nakamura, “Comprehensive prediction of target RNA editing sites for PLS-class PPR proteins in *Arabidopsis thaliana*,” Plant and Cell Physiology, vol. 60, no. 4, pp. 862-874, Apr, 2019.

32. P. Giege, J. M. Grienenberger, and G. Bonnard, “Cytochrome c biogenesis in mitochondria,” Mitochondrion, vol. 8, no. 1, pp. 61-73, Jan, 2008.

33. S. F. Cheng, B. Gutmann, X. Zhong, Y. T. Ye, M. F. Fisher, F. Q. Bai, I. Castleden, Y. Song, B. Song, J. Y. Huang, X. Liu, X. Xu, B. L. Lim, C. S. Bond, S. M. Yiu, and I. Small, “Redefining the structural motifs that determine RNA binding and RNA editing by pentatricopeptide repeat proteins in land plants,” Plant Journal, vol. 85, no. 4, pp. 532-547, Feb, 2016.

34. J. L. Heazlewood, J. Whelan, and A. H. Millar, “The products of the mitochondrial orf25 and orfB genes are F-o components in the plant F1Fo ATP synthase,” Febs Letters, vol. 540, no. 1-3, pp. 201-205, Apr, 2003.

35. K. Hammani, C. C. des Francs-Small, M. Takenaka, S. K. Tanz, K. Okuda, T. Shikanai, A. Brennicke, and I. Small, “The pentatricopeptide repeat protein OTP87 is essential for RNA editing of nad7 and atp1 transcripts in Arabidopsis mitochondria,” Journal of Biological Chemistry, vol. 286, no. 24, pp. 21361-21371, Jun, 2011.

36. T. T. Xie, D. Chen, J. Wu, X. R. Huang, Y. F. Wang, K. L. Tang, J. Y. Li, M. X. Sun, and X. B. Peng, “Growing Slowly 1 locus encodes a PLS-type PPR protein required for RNA editing and plant development in Arabidopsis,” Journal of Experimental Botany, vol. 67, no. 19, pp. 5687-5698, Oct, 2016.

37. T. Pasternak, G. Potters, R. Caubergs, and M. A. K. Jansen, “Complementary interactions between oxidative stress and auxins control plant growth responses at plant, organ, and cellular level,” Journal of Experimental Botany, vol. 56, no. 418, pp. 1991-2001, Aug, 2005.

38. P. Willems, A. Mhamdi, S. Stael, V. Storme, P. Kerchev, G. Noctor, K. Gevaert, and F. Van Breusegem, “The ROS wheel: refining ROS transcriptional footprints,” Plant Physiology, vol. 171, no. 3, pp. 1720-1733, Jul, 2016.

39. G. Potters, T. P. Pasternak, Y. Guisez, and M. A. K. Jansen, “Different stresses, similar morphogenic responses: integrating a plethora of pathways,” Plant Cell and Environment, vol. 32, no. 2, pp. 158-169, Feb, 2009.

40. S. B. Huang, O. Van Aken, M. Schwarzlander, K. Belt, and A. H. Millar, “The roles of mitochondrial reactive oxygen species in cellular signaling and stress response in plants,” Plant Physiology, vol. 171, no. 3, pp. 1551-1559, Jul, 2016.

Figure legends

Fig.1 Effects of the TDF mutations on the early stages of LR development. (A) Fasciated LRs formed at 28°C in the TDF mutant explants versus a normal root on the wild-type (WT) explant after 6 days of culture. **(B)** Schematic representation of LR development (stages I-V). **(C)** Schematic image of a primordium at stage II. The area consisting of more than one cell layer (MOL) is delimited by red lines. **(D)** Stage II primordia formed at 28°C in WT explants and TDF mutant explants. **(E)** Effects of the TDF mutations on the number of cells in the outermost layer of MOL of stage II primordia at 22°C (black) and 28°C (orange). N = 17 to 28. **(F)** Schematic image of a primordium at the transition from stage IV to stage V. The areas consisting of MOL and more than two cell layers (MTL) are delimited by red lines and blue lines, respectively. **(G)** Stage IV–V primordia formed at 28°C in WT explants and TDF mutant explants. **(H)** Scatter plot of the width of MTL versus the width of MOL at 22°C (black) and 28°C (red) as influenced by the TDF mutations. N = 31 to 66. **(I)** LR densities in the WT explants and TDF mutant explants cultured at 22°C or 28 °C (including all developmental stages; mean ± s.d., N = 21 to 29, P > 0.3, ANOVA). Scale bars: 100 µm (**A**), 50 µm (**D**, **G**).

Fig.2 Tissue-specific expression and subcellular localization of the TDF proteins. (A) Protein structures of RRD1, RRD2, and RID4. **(B and C)** Expression of *RRD1::RRD1:GFP* (**B**, left), *RID4::RID4:GFP* (**B**, right), and *35S::Mt-GFP* (**C**) at stage II of LR primordium development. Prodium iodide was used as a red counter-stain. **(D and E)** Expression of *RRD1::RRD1:GFP* (**D**, upper panels), *RID4::RID4:GFP* (**D**, lower panels), and *35S::RRD2:GFP* (**E**) in callus-derived protoplasts. Mitochondria were labelled with Mitotracker Orange. Scale bars: 50 µm (**B and C**), 5 µm (**D and E**).

Fig.3 Accumulation of polyadenylated mitochondrial transcripts in *rrd1*. (A) MA-plot for microarray analysis of poly(A)$^+$ transcripts of *rrd1* versus wild-type (WT) explants that were LR-induced at 28°C for 12h. **(B)** qRT-PCR analysis of explants LR-induced at 28°C for 12h. Total and polyadenylated transcript levels are shown for *cytochrome oxidase subunit 1* (*cox1*)*, cox2, NADH dehydrogenase subunit 6* (*nad6*)*, apocytochrome B* (*cob*)*,* and *ATP synthase subunit 4* (*atp4*) (mean ± s.d., N = 3, *P < 0.05, **P < 0.01, Welch's t-test). **(C)** 3' end analysis of *cox1* mRNA by CR-RT PCR. mRNAs were prepared from WT and *rrd1* seedlings first grown at 22°C for 7 days and then at 28°C for 1 day. The genomic sequence of *cox1* is shown in green. **(D)** RACE-PAT assay showing accumulation of polyadenylated transcripts of *atp8*, *cob*, *cox1*, *cox2*, *nad6*, *nad9*, and *-Tubulin 4 (TUB4)*. mRNAs were prepared from explants LR-induced at 28°C for 12h.

Fig.4 Effects of the *ags1* on the phenotypes of *rrd1*. (A) RACE-PAT assay showing accumulation of polyadenylated transcripts of *cox1* and *TUB4*. *rrd1* mutant strains harboring either *ags1* or *AGS1^c* were obtained by *rrd1* (Ler background) × *ags1* (Col background) and *rrd1* ×Col crosses, respectively. mRNAs were prepared from seedlings grown first at 22°C for 5 days and then at 28°C for 3 days. **(B)** Representative images of LRs formed at 28°C after 6 days of culture (upper panels). Basal width of LRs formed was scored (lower panel, N = 115 to 116 for *rrd1 ags1* and *rrd1 AGS1^c*, N = 22 to 43 for others, **P < 0.01, Mann-Whitney-Wilcoxon test). **(C)** Seedlings grown at 28°C for 13 days. Scale bars: 100 µm (**B**), 2 cm (**C**).

Fig.5 Effects of *rrd2* and *rid4* on mitochondrial mRNA editing and protein synthesis. (A) Sequencing analysis of mitochondrial mRNA editing in explants that were LR-induced at 28°C for 12h.

(B) BN-PAGE analysis of mitochondrial protein complexes. Mitochondria were extracted from seed-derived liquid-cultured callus first incubated at 22°C for 20 days and then at 22°C or 28°C for an additional 3 days. **(C and D)** Immunoblot analysis of cyt c. Mitochondria were extracted in the same conditions as in (B). The results of densitometry analysis are shown in (**D**) (N = 3, mean ± s.d.). **(E and F)** Immunoblot analysis of cyt c using mitochondria extracted from callus cultured first at 22°C for 14 days and then at 28°C for 7 days. The result of densitometry analysis is shown in (**F**) (N = 2, mean ± s.d., **P < 0.01, Welch's t-test)

Fig.6 Fasciated LR formation following treatment with chemicals inhibiting mitochondrial respiration or inducing ROS. (A to D) LRs were induced from the wild type in the presence of rotenone (**A**), antimycin A (**B**), or oligomycin (**C**), and the basal width of LRs formed was scored after 6 days in culture (median, 25% - 75% quantile, N = 30 to 76, *P < 0.05, **P < 0.01, Mann-Whitney-Wilcoxon test). Typical LRs formed in each treatment are shown in (**D**). **(E and F)** LRs were induced from the wild type in the presence of CCCP. The basal width of LRs (**E**, median, 25% - 75% quantile, N = 2 to 53, P > 0.07, ANOVA) and the number of LRs per segment (**F**, Number of segments = 12, **P < 0.01, Welch's t-test) were scored at the 6th day. **(G and H)** The effects of applying ascorbate on wild type, PQ treated, or *rid4-2* segments during LR formation. Basal width of LRs formed was measured at the 6th day of LR induction (**G**, median, 25% - 75% quantile, N = 16 to 58, **P < 0.01, Mann-Whitney-Wilcoxon test). Representative images of LRs in each condition are shown in (**H**). **(I)** *DR5::GUS* expression at 12 h post LR-induction under treatment with NPA or PQ. Scale bars: 100 μm (**D** and **H**), 1 mm (**I**).

Supplemental figure legends

fig. S1 Chromosome mapping of the TDF mutations, *rrd1*, *rrd2*, and *rid4-1*.

(A) Chromosome mapping of the *rrd1* mutation. Black rectangles represent annotation units around the *RRD1* locus on chromosome 3, and red numerals correspond to the numbers of recombination events between DNA polymorphism markers and the *RRD1* locus. The *rrd1* mutation was mapped to the region covered by the annotation units MJL12, MTE24, and MWL2. Sequencing of this region, followed by complementation analysis, identified the *rrd1* mutation as a G to A transition in At3g25430 (orange arrow). **(B)** Chromosome mapping of the *rrd2* mutation. Black rectangles represent annotation units around the *RRD2* locus on chromosome 1, and red numerals correspond to the numbers of recombination events between DNA polymorphism markers and the *RRD2* locus. The *rrd2* mutation was mapped to the region covered by the annotation units F3C3, F27G20, and F5D14. Sequencing of this region, followed by allelism analysis, identified the *rrd2* mutation as a G to A transition in At1g32415 (orange arrow). **(C)** Chromosome mapping of the *rid4-1* mutation. Black rectangles represent annotation units around the *RID4* locus on chromosome 2, and red numerals correspond to the numbers of recombination events between DNA polymorphism markers and the *RID4* locus. The *rid4* was mapped to the region covered by the annotation units F4P9 and T1B8. Sequencing of this region, followed by complementation analysis, identified the *rid4* mutation as a G to A transition in At2g33680 (orange arrow).

fig. S2 Complementation analysis for identification of the TDF genes, RRD1, RRD2, and RID4

(A) Complementation analysis for identification of the *RRD1* gene. The genomic fragment GL07 encompassing At3g25430, where an *rrd1* phenotype-linked mutation was found, was introduced into the wild type and crossed with *rrd1*. Each individual of the F2 progeny was genotyped for the *rrd1* allele and GL07 transgene. Hypocotyl explants of the F2 progeny were cultured on RIM at 28℃ for 14 days and examined for adventitious rooting. The explants were categorized by the lengths of adventitious roots (Short, adventitious root length ≤ 5 mm; Long, adventitious root length ≥ 5 mm) and counted. The result showed that development of adventitious roots, which was highly temperature-sensitive in the *rrd1* mutant, was clearly rescued by the introduction of GL07. Therefore, we concluded that the *RRD1* gene corresponds to At3g25430. **(B and C)** Defect of adventitious root formation in a T-DNA insertion mutant of At1g32415. SALK_027874 carries a T-DNA insertion in the middle of At1g32415 (**B**). The transcribed region and open reading frame of At1g32415 are indicated by the open arrow and grey box, respectively. Hypocotyl explants of Col, L*er*, *rrd2*, and SALK_027874 were cultured on RIM at 28℃ for 27 days and examined for adventitious rooting (**C**). The result indicated that SALK_027874 as well as *rrd2* are defective in adventitious root formation at this temperature. Since adventitious root formation was not much affected at 22℃ in both *rrd2* and SALK_027874 (data not shown), SALK_027874 was shown to be temperature-sensitive for root development as is *rrd2*. Bar = 1cm. **(D)** Allelism test for identification of the *RRD2* gene. The *rrd2* mutant was crossed with SALK_027874 carrying a T-DNA insertion in At1g32415, where an *rrd2* phenotype-linked mutation was found. Each individual of the F2 progeny was genotyped for the *rrd2* and the T-DNA insertion alleles. Hypocotyl explants of the F2 progeny were cultured on RIM at 28℃ for 14 days and examined for adventitious rooting. The explants were categorized by the lengths of adventitious roots (Short, adventitious root length ≤ 5 mm; Long, adventitious root length ≥ 5 mm) counted. The result indicated clearly that *rrd2* and SALK_027874 are allelic. Therefore, we concluded that the *RRD2* gene corresponds to At1g32415. **(E)** Complementation analysis for identification of the *RID4* gene. The genomic fragment GL91321 encompassing At2g33680, where we found an *rid4* phenotype-linked mutation, was introduced into *rid4*, and the resultant transgenic *rid4* mutant harboring GL91321 (*rid4*/GL91321) was used for complementation analysis. Hypocotyl explants of the wild type (WT), *rid4*, and *rid4*/GL91321-2 were cultured on RIM at 28℃ for 19 days and examined for adventitious root formation. Development of adventitious roots, which was highly temperature-sensitive in the *rid4* mutant, was clearly rescued by the introduction of GL91321. Therefore, we concluded that the *RID4* gene corresponds to At2g33680. Bar = 1 cm.

fig. S3 Identification and characterization of the *rid4-2* mutant.

(A) Representative images of LRs formed at 22°C or 28°C in the explants of the wild type or the *rid4-2* mutant after 6 days of culture. Fasciated LRs were observed in *rid4-2* explants at 28°C. **(B)** Phenotypes of seedlings that were grown for 7 days on vertical GMA plates. Seedlings were grown either at 22°C or 28°C. **(C)** Allelism test between *rid4-1* and *rid4-2.* F_1 plants derived from reciprocal crossing between *rid4-1* and *rid4-2* were subjected to phenotypic analysis for AR formation. Hypocotyl explants of *rid4-1*, *rid4-2*, L*er* WT, and F1 plants were cultured on RIM for 24 days at 28°C. **(D)** Chromosome mapping of the *rid4-2* mutation. Black rectangles represent annotation units around the *RID4* locus on chromosome 2, and red numerals correspond to the numbers of recombination events between DNA polymorphism markers and the *RID4* locus. *rid4-2* was mapped to the region covered by the annotation units F4P9 and

T29F13. Sequencing of this region, followed by complementation analysis, identified the *rid4-2* mutation as a G to A transition in At2g33680 (orange arrow). Scale bars: 100 μm (**A**), 1 cm (**B**).

fig. S4 Functionality and expression of *RRD1::RRD1:GFP* and *RID4::RID4:GFP*

(A) Phenotypic complementation of *rrd1* by the introduction of the GFP reporter gene *RRD1::RRD1:GFP*. F3 plants homozygous for rrd1 that had been derived from the cross between rrd1 and Col carrying *RRD1::RRD1:GFP* were phenotyped for AR formation from hypocotyl explants at 28°C and genotyped for the presence of *RRD1::RRD1:GFP* (+, present; -, absent). **(B)** Phenotypic complementation of *rid4* by the introduction of the GFP reporter gene *RID4::RID4:GFP*. *rid4* homozygotes of which the genetic background had been partially replaced by crossing with the Col strrain were tranformed with *RID4::RID4:GFP*. Plants of the resultant T2 line were phenotyped for AR formation from hypocotyl explants at 28°C and genotyped for the presence of *RID4::RID4:GFP* (+, present; -, absent). **(C)** Expression patterns of *RRD1* and *RID4* in the root apical region. GFP signals in the primary roots of the transgenic plants harbouring *RRD1::RRD1:GFP* and *RID4::RID4:GFP* showed strong expression of *RRD1* and *RID4* in the root apical meristem. Scale bar = 100 μm.

fig. S5 Characterization of RRD1 function.

(A to C) Microarray analysis of mitochondrial gene in *rrd1*. MA-plot for microarray analysis of poly(A)$^+$ transcripts of *rrd1* versus wild-type (WT) explants that were LR-induced at 28°C for 12h. Characterized mitochondrial genes are shown in blue, while non-characterized mitochondrial ORFs or pseudogenes are shown in red (**A**). The names of the characterized genes is indicated in (**B**). **(C)** The function and array element ID of the characterized mitochondrial genes in the GeneChip™ Arabidopsis Genome ATH1 Array. **(D and E)** PARN activity assay of RRD1. TALON-purified fraction of total cell lysate with or without IPTG-induction (**D**). PARN activity assay using the TALON-purified fraction **(E)**.

fig. S6 Sequence alignment of RRD1 and PARNs of various organisms.

An alignment of amino acid sequences was generated between RRD1 and PARNs of human, *Xenopus laevis*, and*A. thaliana* by using the ClastalW program and processed with BOXSHADE (http://www.ch.embnet.org/software/BOX_form.html). Identical and similar amino acid residues are highlighted on black and grey backgrounds, respectively. R3H domain is marked by the dotted orange box, and RNA recognition motif (RRM) is marked by the solid blue box. These domains are conserved in the animal PARNs (human and *X. laevis*), but not clearly present in the *A. thaliana* PARN and RRD1. The pink asterisk represents the tryptophan residue of which codon was changed into a stop codon by the *rrd1* mutation. The red arrowheads represent the four residues important for PARN activity (*29*).

fig. S7 Comprehensive analysis of mitochondrial mRNA editing in *rrd2* and *rid4-1*.

Sequencing analysis of mitochondrial mRNA editing was performed using explants that were LR-induced at 28°C for 12h. The color code indicates the level of C-to-U RNA editing at each site (Editing status: -

0.5 = 100% C, 0.5 = 100% U). Presumptive specific editing sites of RRD2 and RID4 are shown is marked by solid blue boxes. RNA editing in *rid4-2* was also analyzed for sites affected in *rid4-1*.

fig. S8 Analysis of mitochondrial mRNA editing in *rrd2* and *rid4-1*.

(A) Sequencing analysis of mitochondrial mRNA editing was performed using explants that were LR-induced at 22°C for 12h. **(B)** Alignment of estimated biding sequence of RRD2 and RID4 (*31*). **(C)** Analysis of mRNA editing of *ccb3* in explants cultured at 22°C or 28°C for 12h.

fig. S9 Effects of NPA and PQ on LR formation.

Root explants 6 days after LR-induction under treatment with NPA or PQ. Scale bar: 1 mm.

table S1. Primers used in this study.

Acknowledgements

We thank T. Nakagawa for providing the binary vector pGW3, M. Sugita for valuable discussion on the PPR proteins, H. Sakurai for the technical support of the *35S::RRD2:GFP* expression in protoplasts, W. Sakamoto and S. Arimura for providing the *35S::Mt-GFP* line, Y. Otsuka and Y. Kondo for the assistance on GFP imaging, S. Endo and H. Morinaka for the assistance on qRT-PCR. This work was supported by Grants-in-Aid for Scientific Research on Priority Areas (No. 19060001 to M.S. and No. 19060016) and Grant-in-Aid for Scientific Research (B) (No. 25291057 to M.S.) from the Ministry of Education, Culture, Sports, Science and Technology, Japan and also by a Grant-in-Aid for JSPS Fellows (No. 218676 to K.O. and No. 17J05722 to A.M.) from the Japan Society for the Promotion of Science.

Author contributions

K.O. designed and performed the experiments, analyzed data, and wrote the manuscript. A.M. designed and performed the experiments, analyzed data, and wrote the manuscript. M.K. identified *RID4* by positional cloning. M.N. designed and performed analysis of PARN activity of recombinant RRD1. A.K. conducted chromosome mapping of *rrd1* and some of the initial characterization of the TDF phenotype. H.T. isolated the *rid4-2* mutant. M.A. and M.Sa. conducted chromosome mapping of *rid4-2*. K.Y. collected preliminary data on the genetic relationship between *rrd1* and *ags1*. T.Ha. and K.N. contributed to the research design and data interpretation for mitochondrial respiration-related analysis. T.U. contributed to the research design, imaging analysis of GFP reporters, and data interpretation for subcellular localization. Y.Y., T.N., and K.Y. performed preliminary analysis of RNA editing. Y.Y., T.K., and T.N. contributed to the research design and data interpretation for RNA editing-related analysis. Y.S. contributed to the analysis of the recombinant RRD1 protein. T.Hi. contributed to the research design and data interpretation for RNA metabolism-related analysis. M.Su. directed the study, conducted preliminary experiments, and wrote the manuscript. All authors read and approved the paper.

Author information

The authors declare no competing financial interests. Correspondence and requests for materials should be addressed to M.S. (sugiyama@ns.bg.s.u-tokyo.ac.jp).

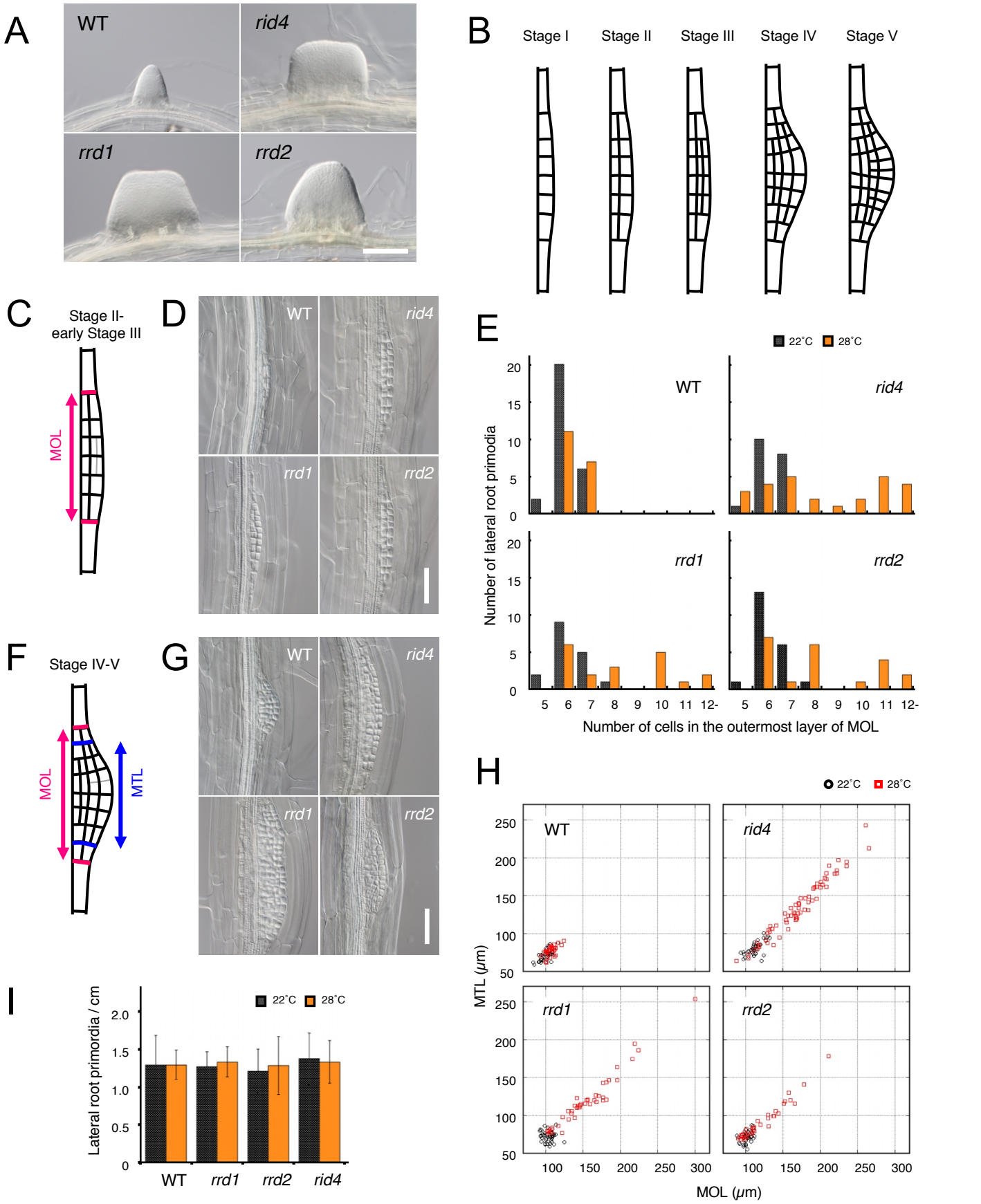

Fig. 1

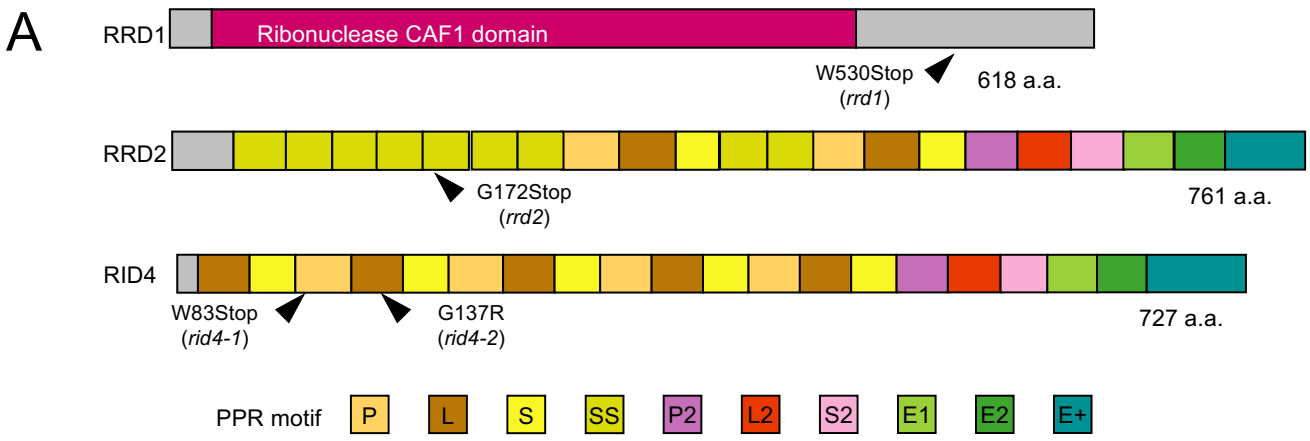

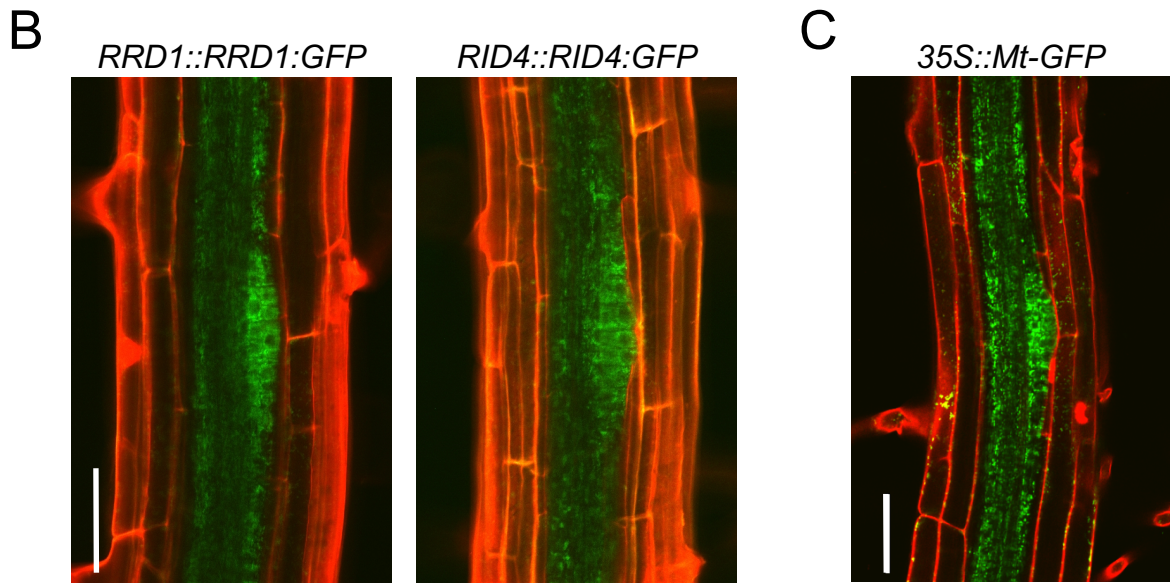

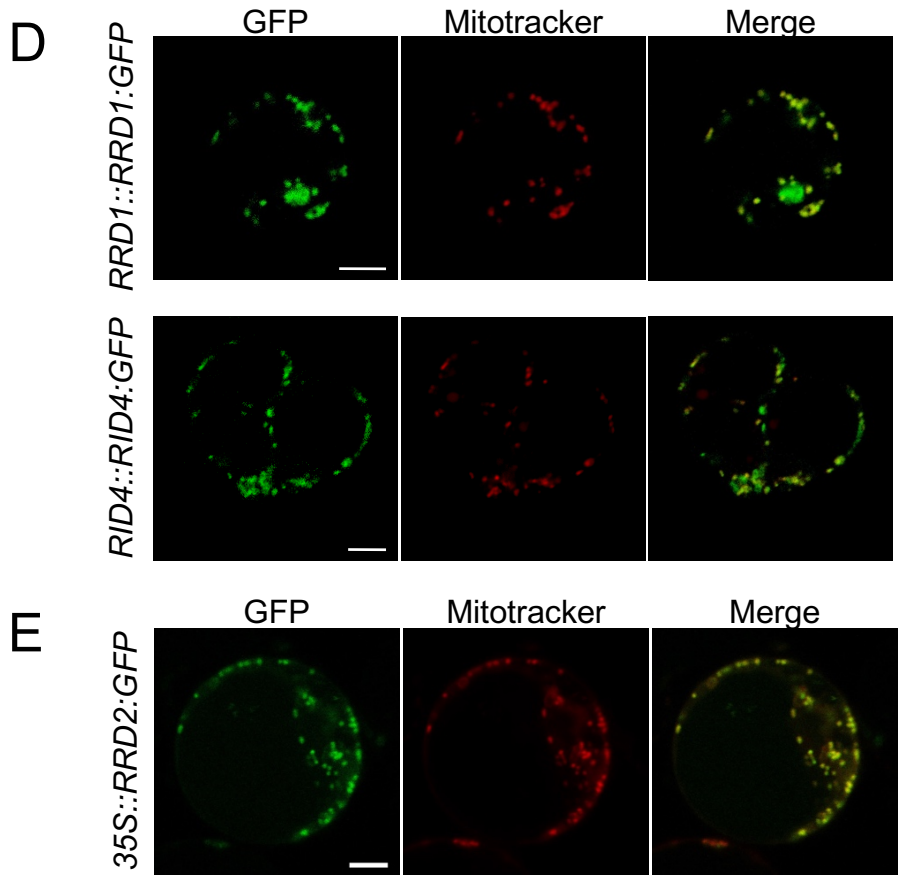

Fig. 2

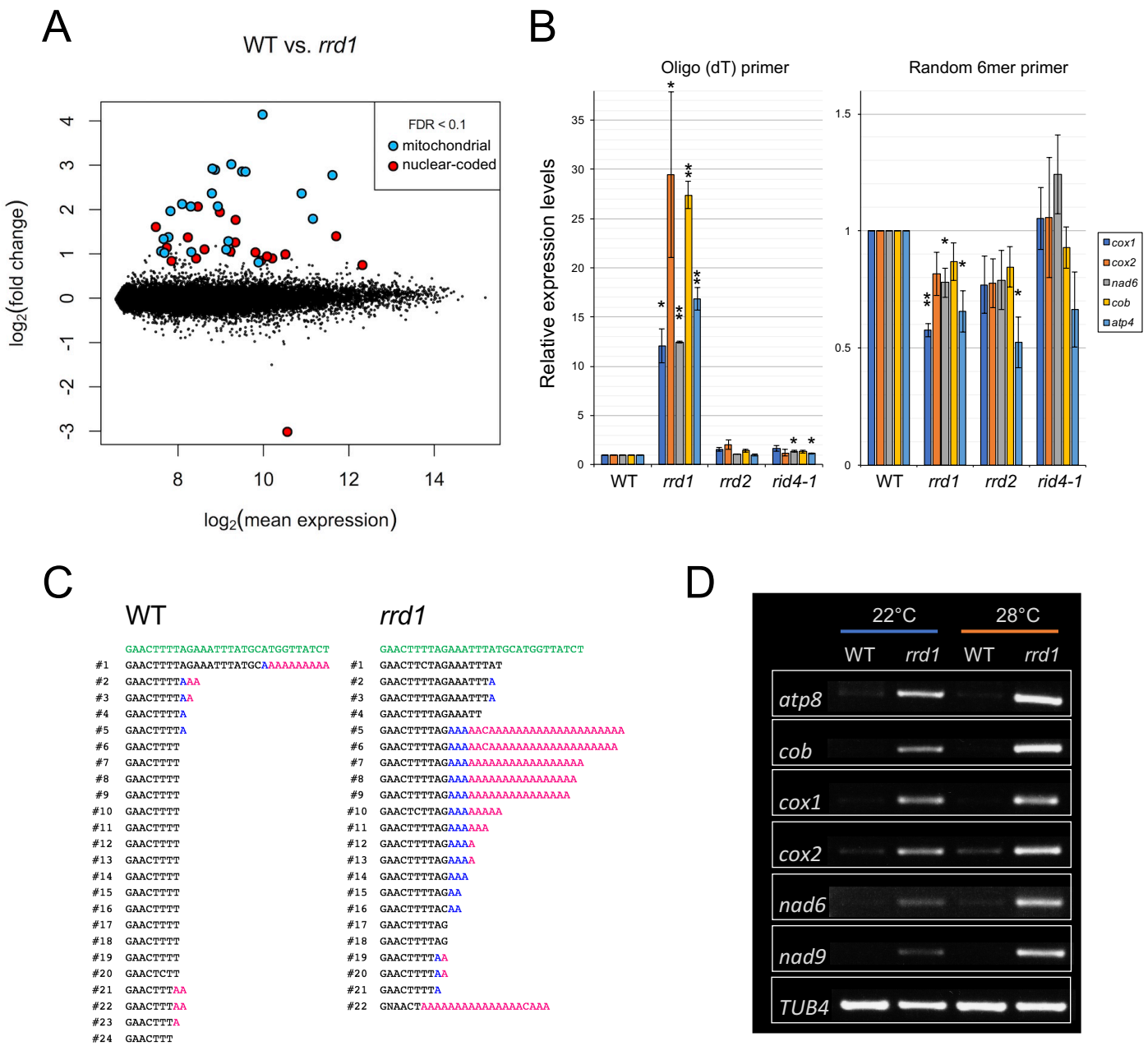

Fig. 3

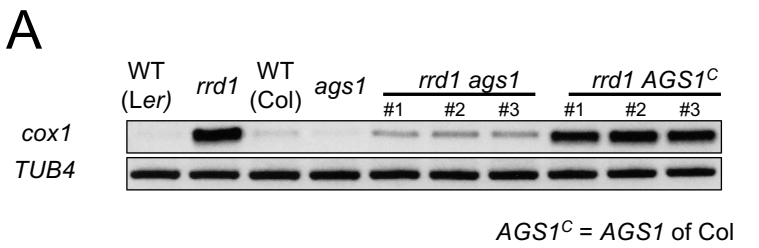

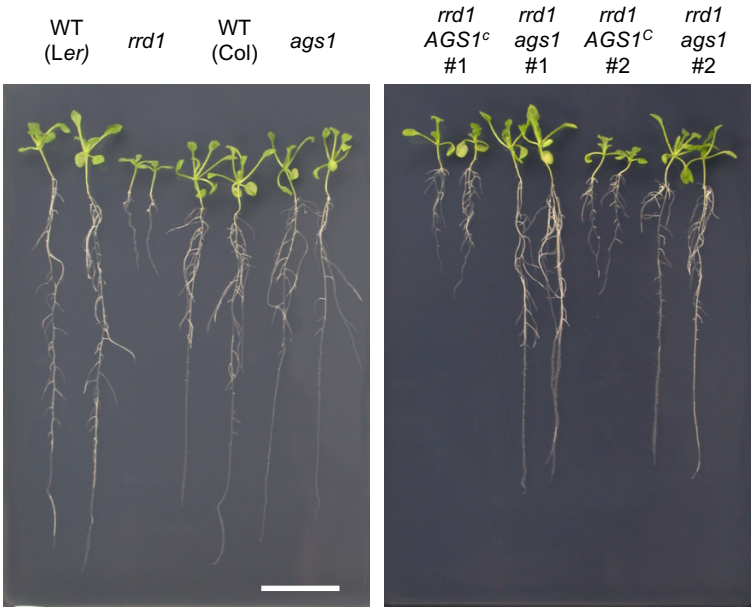

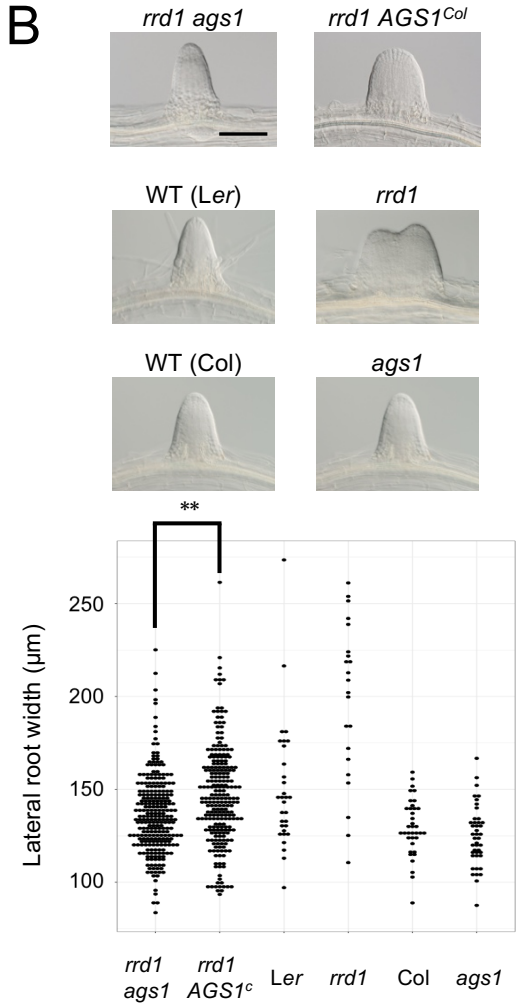

Fig. 4

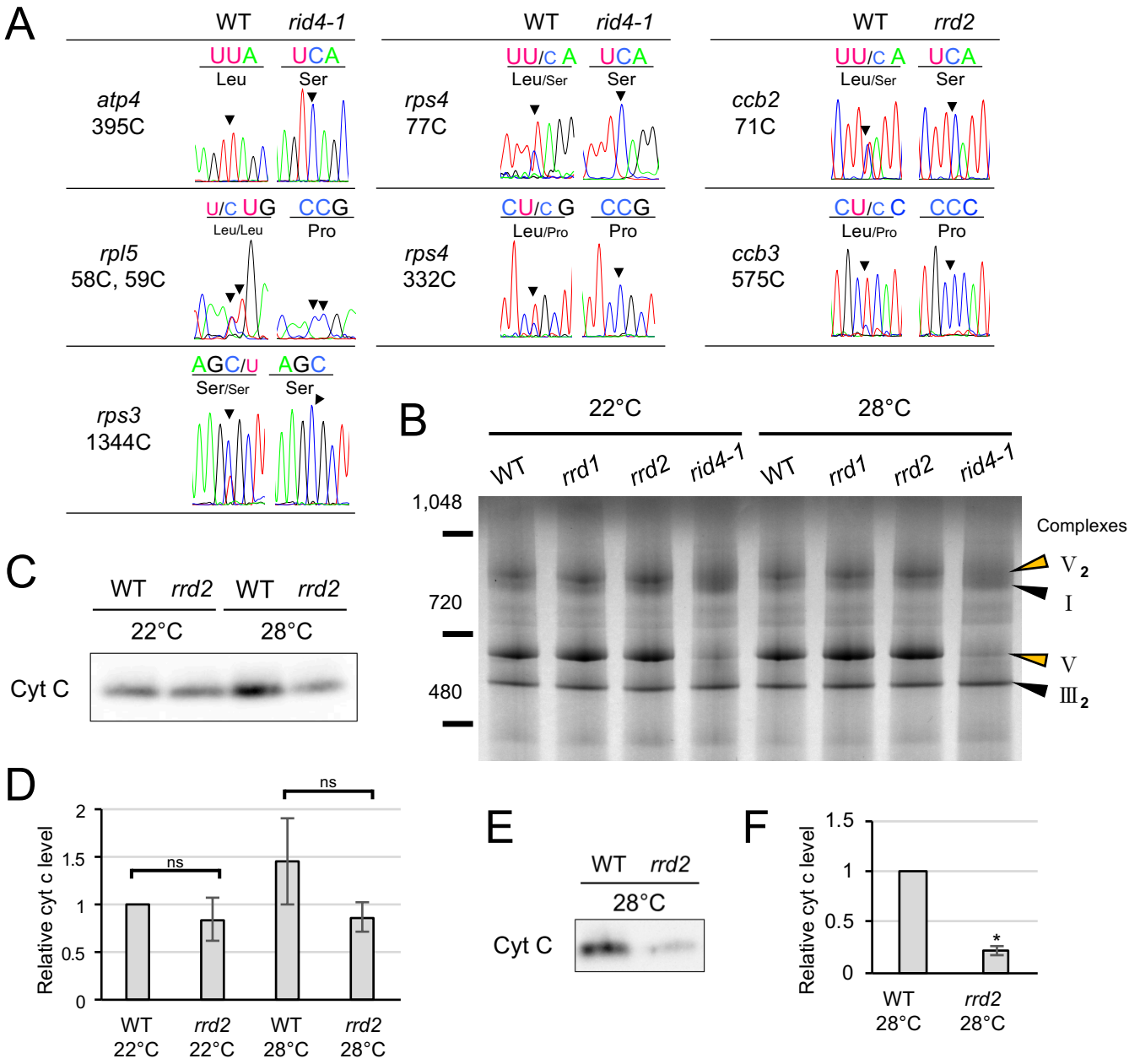

Fig. 5

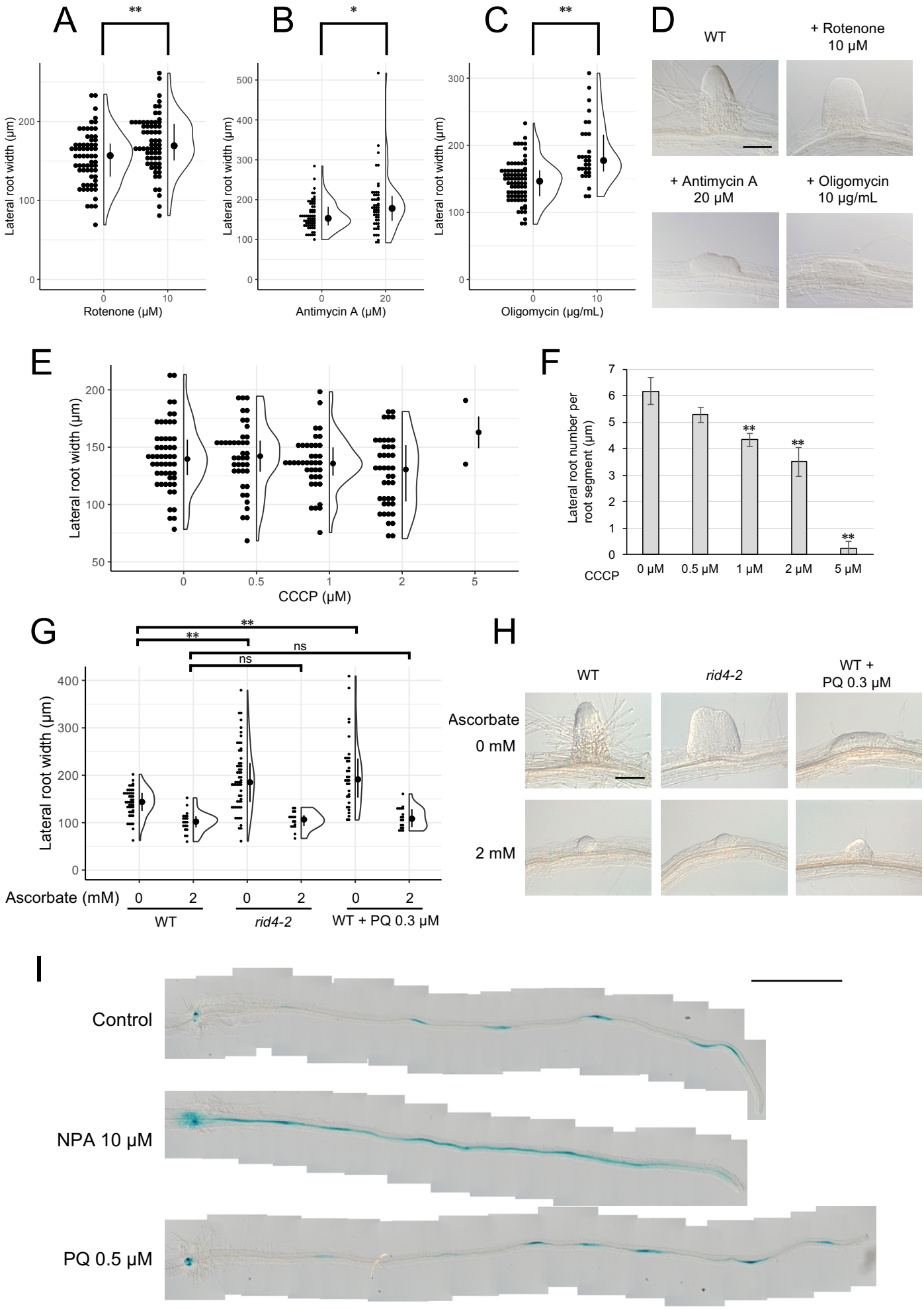

Fig. 6